



## OPEN ACCESS

## EDITED BY

Muhammad Faisal Manzoor,  
Foshan University, China

## REVIEWED BY

Xiaohui Lin,  
University College Dublin, Ireland  
Seyed-Hassan Miraei Ashtiani,  
Dalhousie University, Canada

## \*CORRESPONDENCE

Xia Zheng  
✉ zx\_mac@shzu.edu.cn

RECEIVED 21 October 2023

ACCEPTED 15 December 2023

PUBLISHED 08 January 2024

## CITATION

Yang T, Zheng X, Xiao H, Shan C and  
Zhang J (2024) Online monitoring system of  
material moisture content based on the Kalman  
filter fusion algorithm in air-impingement dryer.  
*Front. Sustain. Food Syst.* 7:1325367.  
doi: 10.3389/fsufs.2023.1325367

## COPYRIGHT

© 2024 Yang, Zheng, Xiao, Shan and Zhang.  
This is an open-access article distributed under  
the terms of the [Creative Commons Attribution  
License \(CC BY\)](https://creativecommons.org/licenses/by/4.0/). The use, distribution or  
reproduction in other forums is permitted,  
provided the original author(s) and the  
copyright owner(s) are credited and that the  
original publication in this journal is cited, in  
accordance with accepted academic practice.  
No use, distribution or reproduction is  
permitted which does not comply with these  
terms.

# Online monitoring system of material moisture content based on the Kalman filter fusion algorithm in air-impingement dryer

Taoqing Yang<sup>1,2,3</sup>, Xia Zheng<sup>1,2,3\*</sup>, Hongwei Xiao<sup>4</sup>, Chunhui Shan<sup>5</sup>  
and Jikai Zhang<sup>1,2,3</sup>

<sup>1</sup>College of Mechanical and Electrical Engineering, Shihezi University, Shihezi, China, <sup>2</sup>Key Laboratory of Northwest Agricultural Equipment, Ministry of Agriculture and Rural Affairs, Shihezi, China, <sup>3</sup>Key Laboratory of Modern Agricultural Machinery Corps, Shihezi, China, <sup>4</sup>College of Engineering, China Agricultural University, Beijing, China, <sup>5</sup>College of Food, Shihezi University, Shihezi, China

A Kalman filter fusion algorithm was proposed, and an online monitoring system was developed for real-time monitoring of the moisture content of materials in an air-impingement dryer. The Kalman filter algorithm was used to estimate the optimal state of the original detection values of the weighting sensor and air velocity sensor. A backpropagation (BP) neural network fusion model was established, where the weight detection value, elastic substrate temperature, air velocity, and impingement distance were considered inputs and the real weight of the material was the output. The optimal topology of the BP neural network was selected, and the initial weights and thresholds of the BP neural network were optimized using a genetic algorithm. The coefficient of determination ( $R^2$ ) and root mean square error (RMSE) of the optimized BP neural network fusion model were 0.9995 and 4.9, respectively. The Kalman filter fusion algorithm, which can realize online monitoring of moisture content, was established using the Kalman filter algorithm and fusion model. Moreover, an online monitoring system for material moisture content was developed, validation experiments were carried out, and the  $R^2$  and RMSE of the nine sets of validation experiments were 0.9963 and 0.78, respectively. The monitoring system satisfied the requirements of material moisture content detection accuracy in the drying process. The developed monitoring system is greatly important for improving the automation level of the drying equipment for fruits and vegetables. The proposed Kalman filter fusion algorithm also provides a reference for other multifactor fusion detection.

## KEYWORDS

online monitoring, moisture content, Kalman filter, neural network, fusion model

## 1 Introduction

Food security and storage have always been one of critical challenges worldwide, especially for fruits and vegetables, which have severe postharvest losses (Zartha Sossa et al., 2021). At present, one of the best ways to solve this problem is drying. By reducing the moisture content to a safe level, drying can significantly minimize deterioration due to microbial conditions, extend the shelf life of products, reduce the cost of packaging, transportation, and storage, and

effectively reduce postharvest losses (Xiao and Mujumdar, 2020). Air-impingement drying technology realizes drying through the impact and heating of hot air on the material; it is crucial for post-harvest drying treatment of agricultural products. Air-impingement drying technology is characterized by a high drying rate and high heat transfer coefficient (Yang et al., 2023) and has been widely used in the drying process of kumquat (Tan et al., 2022), tomato (Tan et al., 2021), kiwifruit (Li et al., 2023), apple (Peng et al., 2019), shiitake mushroom (Liu et al., 2020), and other agricultural products.

Moisture content is a critical parameter in air-impingement drying and other drying processes, and its online monitoring plays a vital role in improving the drying automation level, optimizing the drying process, and ensuring the continuity of drying. Existing online moisture content detection methods include the model prediction method (Dalvi-Isfahan, 2020), dielectric properties method (Celik et al., 2022), hyperspectral imaging method (Cho et al., 2020), nuclear magnetic resonance method (Li et al., 2021), and weighing method (Pongsuttiyakorn et al., 2019). The model prediction and dielectric characterization methods only apply to the moisture content detection of the same material in a fixed drying condition and require improved versatility. Hyperspectral imaging and nuclear magnetic resonance methods cannot be applied to agricultural drying products with low added value due to their high cost and complex operation steps. The weighing method is not limited by the type of material and drying condition and is more versatile. At the same time, it is widely used for online monitoring of moisture content in the drying process of fruits and vegetables due to its low cost and simple operation.

The weighing method utilizes the oven method to obtain the initial moisture content of a batch of materials (Wang et al., 2022). Under the premise of defaulting to the same batch of materials with the same initial moisture content, based on the principle of a constant mass of dry matter in the drying process, the weighing method converts the material's weight in the drying process into moisture content. The key to realizing accurate detection of moisture content of materials in the drying process by weighing method is the accurate measurement of real-time weight of materials using a weighting sensor. The uncertainty of the drying environment caused substantial difficulties in realizing the accurate measurement of material weight. The impact of the airflow on the weighing tray during the drying process directly and remarkably affects the detection results of the weighting sensor (Xie et al., 2018). Moreover, in different drying processes with different set values of airflow velocity, the influence of airflow on the moisture content detection results is not fixed. The weighting sensors used for online monitoring of moisture content are mostly resistance strain pressure sensors. Variation in the temperature of the sensor's elastic substrate can cause many errors in the detection results of the weighing sensor given some unique properties of this sensor (Xue et al., 2018). The variation of temperature in the existing drying process of fruits and vegetables is roughly in the range of 40°C–70°C. The effect of drying temperature on the material weight detection results becomes nonlinear and complex to correct due to the considerable temperature difference. In addition, airflow disturbances and equipment vibrations cause fluctuations in the detection value of the weighting sensor with considerable noise.

To address these problems, Ju et al. (2023), Yang et al. (2023), and Wang et al., 2014 stopped the equipment operation while performing

the material moisture content detection. This method effectively avoided the influence of airflow and equipment vibration on material weight detection. The moisture content of the material in the drying process must be detected more frequently with the development of the drying process and the improvement of drying automation. In this context, the equipment-stop detection program seriously damages the continuity of the material drying process, and ensuring the quality of dry products becomes challenging. To address the nonlinear effect of drying temperature on the measurement results of the weighting sensor, Reyer et al. (2022) installed the weighting sensor outside the drying chamber, thereby fundamentally solving the problem. However, this solution destroyed the drying chamber structure, affected the sealing of the drying chamber, and increased the difficulty of temperature and humidity control in the drying chamber.

The air-impingement drying process can be optimized by varying the distance between the air nozzle and the material, i.e., the impingement distance. Pre-experimentation found that the impingement distance significantly affected the weighting sensor's detection value. In summary, the real-time moisture content detection of the material in the drying process is affected by the weight detection value, the elastic substrate temperature, the airflow velocity, and the impingement distance. A complex nonlinear relationship exists between the material moisture content and the four factors. Machine learning can model the complex nonlinear relationship between the variables. Backpropagation (BP) neural network, a type of machine learning, has been widely used in the fields of drying process modeling (Liu et al., 2020), trajectory prediction (Zheng et al., 2023), fault diagnosis (Wang et al., 2023), and residual life prediction (Ji et al., 2023) because of its powerful nonlinear mapping ability. The BP neural network can be used to build a nonlinear model with weight detection value, elastic substrate temperature, air velocity, and impingement distance as inputs and the real weight of the material as output, resulting in an accurate prediction of the moisture content of the material during the drying process.

The weight of the material, the temperature of the elastic substrate, and the air velocity can be detected sequentially by weighting, temperature, and air velocity sensors. Many fluctuations and noise are observed in the detection values of the three sensors, especially the weighting and air velocity sensors, due to the airflow disturbance, equipment vibration, and the sensors' limitations. Therefore, the raw signals obtained from the sensors should be filtered prior to building the moisture content prediction model. Kalman filter is an efficient autoregressive filter that can estimate the state of the dynamic system in the information, where many uncertainty situations exist and can make an optimal estimation of the detected values of the three sensors mentioned above (Li et al., 2022).

Aiming at these problems, the Kalman filter fusion algorithm was proposed. The Kalman filter algorithm was used to make an optimal estimation of the measured values of the weight sensor, air velocity sensor, and temperature sensor at the same moment. Then, the BP neural network was used to establish a fusion model among the optimal estimation of the three sensors, the impingement distance, and the real weight of the material. Combined with the initial moisture content of the material, the online detection model of moisture content of the material was established, and the Kalman filter fusion algorithm was completed. The online monitoring system of material moisture content was built using this algorithm.

In summary, this study aims (1) to build an information acquisition system of material moisture content in the air-impingement dryer and to obtain the training data used to establish the Kalman filter fusion algorithm; (2) to develop an optimal state estimation of the original monitoring data of the three types of sensors by using the Kalman filter algorithm; (3) to train the BP neural network, and to establish a fusion model with the weight detection value, elastic substrate temperature, air velocity, impingement distance as inputs, and the real weight of the material as outputs; (4) to build an online monitoring system for moisture content and complete the validation experiments of online moisture content detection. This study is expected to realize the online monitoring of the moisture content of materials in air-impingement drying for fruits and vegetables.

## 2 Principles and methods

### 2.1 Operating principle of air-impingement dryer

The centrifugal fan realized the internal air circulation in the inner and outer chambers. The air passing through the nozzles was squeezed into a high-pressure stream, impacting the material on the trays. The infrared tube installed in the upper part of the inner chamber heated the materials on the tray. The material was dried under the double effect of airflow impact and heating. The wet air was discharged through the moisture drain valve in the outer chamber. The operation principle of the air-impingement dryer is shown in Figure 1.

A temperature sensor detected the temperature of the hot air at the nozzle. The closed-loop adjustment of the hot air temperature was realized by adjusting the power of the infrared tube. The detection result of the thermosensitive air velocity sensor was greatly affected by temperature. Thus, accurate detection of the airflow velocity in the drying inner chamber is difficult at different drying temperatures.

Consequently, the centrifugal fan realized the open-loop control of wind speed by adjusting the frequency of the inverter (Yang et al., 2023). The open-loop control of the centrifugal fan also obtained an unstable airflow in the inner chamber.

In the air-impingement drying process, in addition to the drying temperature and air velocity, the tray position was an essential parameter for process optimization (Chang et al., 2022). The positions of the tray in the material rack, the temperature of the material surface, and the air velocity were different, as well as the final quality of the dry products obtained.

### 2.2 Principle of material moisture content detection based on the weighing method

The material moisture content detection prerequisite, based on the weighing method, was obtaining the material's initial moisture content. The dry matter mass of the material  $m_d$  was obtained after the material was continuously dried in a hot air dryer at a drying temperature of 105°C for 24 h (Zahoor et al., 2022). The initial moisture content of the material (wet basis) was calculated from Equation 1 (Liu et al., 2021).

$$W_0 = \frac{m_0 - m_d}{m_0} \times 100\% \tag{1}$$

where  $W_0$  was the initial moisture content of the material, %;  $m_0$  was the initial weight of the material, g;  $m_d$  was the dry matter mass of the material, g.

Material moisture content detection based on the weighing method defaulted to the same batch of material with the same initial moisture content. It converted the real-time weight of the material in the drying process to the moisture content of the material. The formula for calculating the real-time moisture content (wet basis) of the material is as follows:

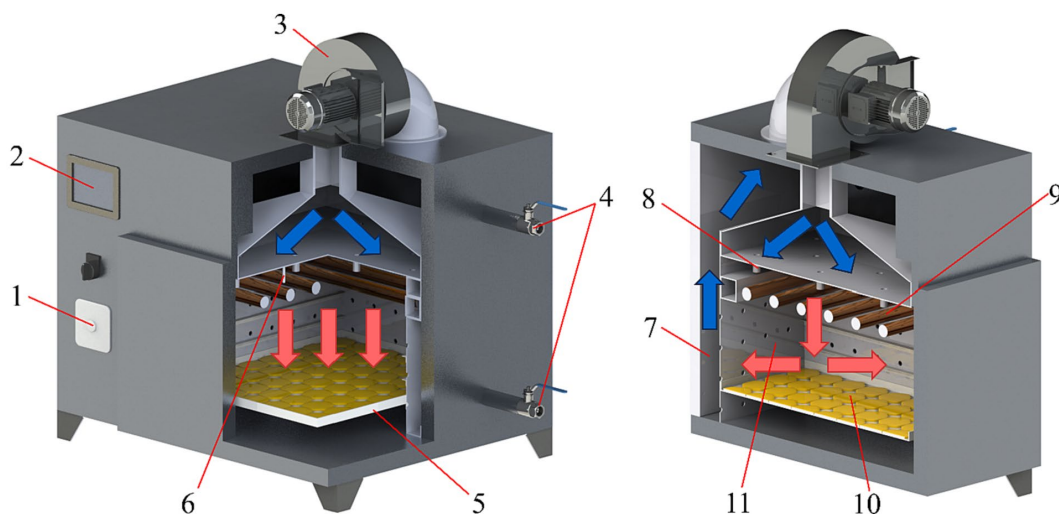


FIGURE 1 Operation principle diagram of air-impingement dryer. (1) Air velocity regulating switch; (2) touch panel; (3) centrifugal fan; (4) moisture drain valve; (5) tray; (6) temperature sensor; (7) outer chamber; (8) air nozzle; (9) infrared tube; (10) material; (11) inner chamber.

$$W_t = \frac{m_t - m_0(1 - W_0)}{m_t} \times 100\% \quad (2)$$

where  $W_t$  is the wet base moisture content of the material at time  $t$ , %;  $m_t$  is the weight of the material at time  $t$ , g.

The above principle indicates that the accurate detection of material weight by the weighing sensor is the core to ensure the accuracy of moisture content detection based on the weighing method. According to the previous experiment and theoretical analysis, air velocity, weighing sensor elastic substrate temperature, impingement distance, and equipment vibration affect the detection of the weighing sensor. Among them, equipment vibration only caused fluctuation and noise to the measurement value of the weighing sensor without direct influence. Airflow disturbances also exacerbated the instability of the weighing sensor measurements.

### 2.3 Information acquisition of material moisture content

The information acquisition system of material moisture content was built to obtain the training data for the Kalman filter fusion algorithm. The information acquisition system utilized the weighing sensor, air velocity sensor, and temperature sensor to collect the raw data of material weight detection value, elastic substrate temperature, and air velocity, respectively. The flow of material moisture content information acquisition is shown in Figure 2.

#### 2.3.1 Information acquisition system of material moisture content

The weighing sensor was installed at the bottom of the material rack and was used to detect the real-time weight of the material. The weighing sensor was a resistance strain pressure sensor (HYPX017, Hengyuan Sensor Technology Co., Ltd., Bengbu, China) ranging from

0–3 Kg. The temperature of the outer chamber was significantly lower than that of the inner chamber due to the lack of heating from the infrared tube. The air velocity sensor was installed in the outer chamber to avoid the influence of temperature on the measured value of the air velocity sensor. The thermosensitive air velocity sensor (WM4200, Chaozhi Reed Technology Co., Ltd., Changchun, China) has a range of 0–20 m/s. A temperature sensor was used to detect the temperature of the elastic substrate of the weighing sensor. A thermally conductive silicone was used to bond the temperature sensor to the elastic substrate. The temperature sensor was a thermocouple-type (PT100, Songguide Heating Sensor Co., Ltd., Shanghai, China) with a range of  $-45^{\circ}\text{C}$ – $125^{\circ}\text{C}$ . All three sensors communicated with the host computer by RS485 module. The upper computer was a Legion Y7000P computer from Lenovo, which was responsible for collecting and storing material moisture content information.

#### 2.3.2 Experimental design of information acquisition of material moisture content

The information acquisition experiments of material moisture content were carried out under different drying process parameters to ensure the accuracy of the Kalman filter fusion algorithm. The range of drying process parameters was initially defined, and that of drying temperature for fruits and vegetables was generally  $40^{\circ}\text{C}$ – $70^{\circ}\text{C}$ . An extremely temperature reduces the drying rate and significantly increases the total energy consumption of the equipment. An extremely high temperature causes the material to produce scorching, browning, and other phenomena, significantly reducing the quality of dry products (Espinoza-Espinoza et al., 2023). The air velocity in the outer chamber was 16 m/s when the centrifugal fan operated at the maximum output wind speed. The minimum air velocity was set to 4 m/s to prevent the phenomenon of low drying rate caused by extremely low air velocity. The structure of the material rack determined the impingement distance. Three layers of material racks are available, and the distance of each layer from the nozzle was 80,

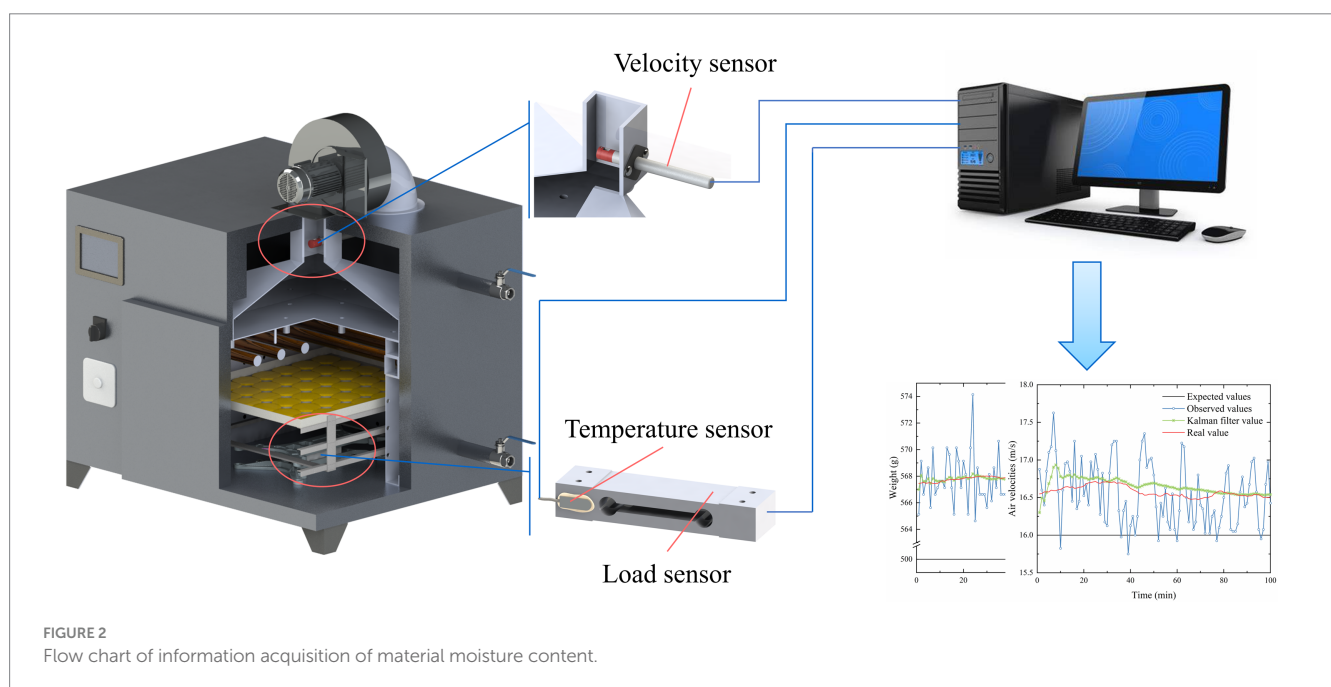


FIGURE 2  
Flow chart of information acquisition of material moisture content.

120, and 160 mm. In summary, the information acquisition experiments of material moisture content were carried out at different drying temperatures (40°C, 50°C, 60°C, and 70°C), different air velocities (4, 8, 12, and 16 m/s), and different impingement distances (80, 120, and 160 mm), totaling 48 groups of experiments (4 × 4 × 3). In each group of experiments, the information acquisition period of material moisture content was 1 min.

Fresh cantaloupe (variety Xizhou Honey No. 17), free from pests, diseases, and damage, was selected as the experimental material. After being peeled and deseeded, the cantaloupe was cut into 30 × 50 × 7 mm slices for drying experiments. The average initial moisture content of fresh cantaloupes was 90.16 ± 1.02% (wet basis).

## 2.4 Kalman filter processing of sensor data

Equipment vibration and airflow disturbance affected the weighting sensor detection signal, and its noise was the most serious. The air velocity sensor was affected by the uncertainty of the dry environment; coupled with the limitations of the sensor, its detection signal had considerable noise and fluctuations. Noise in the detection signals of the two sensors was difficult to avoid. The original detection signals of the two sensors should be filtered prior to data fusion.

The temperature of the elastic substrate of the weighting sensor was less affected by the radiation of the infrared heating tube given that the weighting sensor was mounted on the bottom of the pallet. Changes in the elastomeric substrate temperature were caused by heat conduction with the air in the inner chamber, achieving a relatively stable elastic substrate temperature without significant fluctuations. Preliminary experiments revealed that the detected value of the elastic substrate temperature was 70 ± 0.5°C during the constant temperature drying process at 70°C. Therefore, in this study, only the detection data of the weight sensor and air velocity sensor were subjected to Kalman filtering.

Kalman filtering algorithm is developed for optimal state estimation of a linear system using the equation of the system state and the observed data of the system's current state (You et al., 2022). The optimal estimation can also be considered a filtering process because the observation data include a large amount of noise and disturbance. The Kalman filtering algorithm can reduce the random measurement errors caused by the sensor's limitations during the sensor data acquisition process and the noise pollution caused by uncertain environmental factors. Kalman filtering carries out the next operation using the results of the previous operation without storing the data; its operation cycle is short and is suitable for the real-time state estimation process (Yang et al., 2021). Kalman filtering can update and process the data collected in the field in real-time. It can be used to estimate state variables that cannot be accurately measured by the system.

The flow of the Kalman filter algorithm can be divided into two phases: the prediction update phase and the observation update phase. In the prediction update phase, the current state was predicted using the previous moment state estimate. In the observation update phase, the observed value of the current state was used to correct the predicted value in the prediction update phase to obtain a relatively accurate state estimate of the current moment.

The discrete equation of state for the linear system was initially established, as follows:

$$x(k) = Ax(k-1) + w(k-1) \quad (3)$$

$$y(k) = Hx(k) + v(k) \quad (4)$$

where  $x(k)$  is the state vector of the system;  $A$  is the state transfer matrix;  $y(k)$  is the observation value;  $H$  is the observation matrix;  $w(k)$  and  $v(k)$  are the process noise and observation noise, respectively.

In the prediction update phase, the system state at time  $k$  was predicted based on the system state at time  $k-1$ , as follows:

$$x(k|k-1) = Ax(k-1) \quad (5)$$

where  $x(k|k-1)$  is the state prediction result at time  $k$ ;  $x(k-1)$  is the optimal state estimate at time  $k-1$ .

The covariance of the system at time  $k$  should also be forecasted during the prediction update phase of the system, as follows:

$$P(k|k-1) = AP(k-1)A^T + Q \quad (6)$$

where  $P(k|k-1)$  is the prediction of the covariance of the system at time  $k$ ;  $P(k-1)$  is the covariance of the system at time  $k-1$ , and  $Q$  is the covariance of the system process noise.

In the observation update stage, the Kalman gain  $K_g(k)$  at time  $k$  was initially computed using the prediction covariance at time  $k$  and the covariance  $R$  of the observation error  $v(k)$ , as follows:

$$K_g(k) = P(k|k-1)H^T \left( HP(k|k-1)H^T + R \right)^{-1} \quad (7)$$

Finally, the optimal state estimate  $x(k)$  at time  $k$  was obtained, as follows:

$$x(k) = x(k|k-1) + K_g(k)(y(k) - Hx(k|k-1)) \quad (8)$$

Corrections were made to  $x(k)$  to obtain the real value at moment  $k$ :

$$\hat{x}(k) = Ax(k) + w(k) \quad (9)$$

The covariance of the system at time  $k$  was also updated for the next Kalman filter run, as follows:

$$P(k) = (I - K_g(k)H)P(k|k-1) \quad (10)$$

where  $I$  is the unit matrix. When the system entered the time  $k+1$ ,  $P(k)$  is equal to  $P(k-1)$ , and the Kalman filter continued running until the end of the process.

## 2.5 Fusion modeling

Kalman filtering of sensor detection data provided statistically accurate and valid data for data fusion. This study used a BP neural network for data fusion of weight detection value, elastic substrate temperature, air velocity, and impingement distance. Moreover, the Kalman filter fusion algorithm was established. The flowchart of the Kalman filter fusion algorithm is shown in Figure 3. Furthermore, a fusion model based on partial least squares regression (PLSR) and support vector machine (SVM) was developed and compared with the BP neural network fusion model, and the effectiveness of the BP neural network fusion model was further verified.

### 2.5.1 BP neural networks

BP neural network, one of the most widely used neural network models, can learn and store many mapping relationships between inputs and outputs (Liu et al., 2020). In this study, the BP neural network was used to establish a fusion model, where the actual weight of the material is the output, and to accurately predict the moisture content of the material. The topology of the BP neural network model consisted of three layers of neurons and two activation functions between the three layers of neurons, as shown in Figure 4. The input layer had four neurons, representing the weight detection value, elastic substrate temperature, airflow velocity, and impingement distance. The output layer had only one neuron, representing the actual weight of the material. The number of neurons in the hidden layer must be obtained by trial and error. The activation function between the input and hidden layers is usually nonlinear, including the logsig and transig functions. The transfer function between the hidden and output layers is usually linear (Pureline) (Yang et al., 2023). The optimal topology of the network, i.e., the number of neurons in the hidden layer and the activation function between the input layer and the hidden layer, should be determined to improve the generalization

ability of the model and reduce the training time of the network (Liu et al., 2020).

$$j < n - 1 \tag{11}$$

$$j < \sqrt{m + n} + a \tag{12}$$

$$j = \log_2 n \tag{13}$$

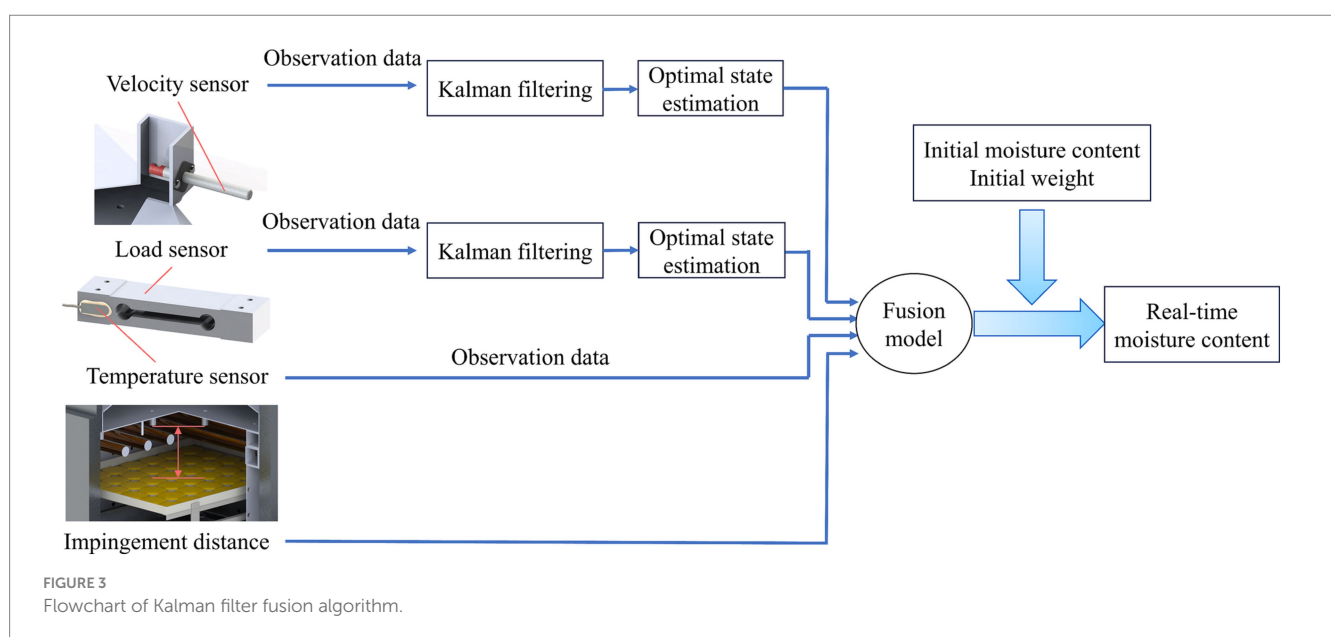
$$j = 2n + 1 \tag{14}$$

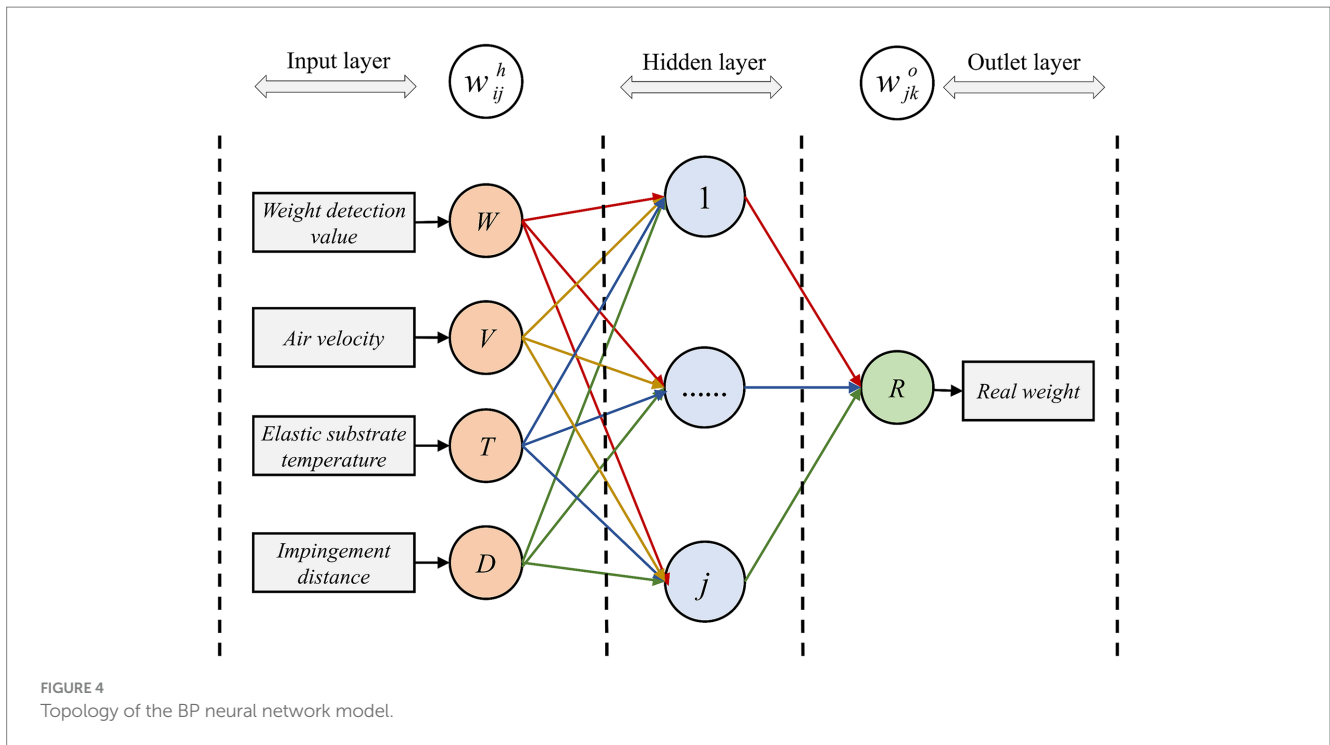
where  $n$  is the number of neurons in the input layer,  $m$  is the number of neurons in the output layer,  $j$  is the number of neurons in the hidden layer, and  $a$  is a constant from 0–10.

The number of neurons in the hidden layer ranged 2–12 based on the union of Equations 11–14 (Martin and Howard, 2002). The optimal topology of the neural network was determined based on the root mean square error (RMSE) and the coefficient of determination ( $R^2$ ) of the model test set (Kalathingal et al., 2020). The  $R^2$  and RMSE were calculated using Equations 15 and 16, respectively.

$$R^2 = 1 - \frac{\sum_{i=1}^n (\hat{y}_i - y_i)^2}{\sum_{i=1}^n (y_i - y_m)^2} \tag{15}$$

$$RMSE = \sqrt{\frac{\sum_{i=1}^n (\hat{y}_i - y_i)^2}{n}} \tag{16}$$





Where  $n$  is the number of data groups in the set,  $y_i$  and  $\hat{y}_i$  are the real value and predicted value of the  $i^{th}$  data groups, and  $y_m$  is the mean value of all the data groups.

Neural networks underwent network training after obtaining the optimal topology. The essence of neural network training was the optimization of weights and thresholds. The initial weights and thresholds of the neural network were randomly generated. However, the training results of the neural network were sensitive to the initial weights and thresholds. A genetic algorithm with global optimization characteristics was used to optimize the initial weights and thresholds of the neural network to ensure the accuracy and generalization ability of the model (Raj and Dash, 2020). The neural network was trained based on the optimized initial weights and thresholds.

Ten data groups were randomly selected from each set of information acquisition experiments of material moisture content, totaling 480 groups of data ( $48 \times 10$ ) for the training of the fusion model. Each group of data included four input variables and one output variable. A total of 480 groups of data were randomly sorted to ensure the reliability of the training results: 70% of the data were used as training data, 15% as validation data, and 15% as test data.

### 2.5.2 Partial least squares regression

The central idea of PLSR is to maximize the synergistic explanation of the relationship between the independent and dependent variables by finding one or more latent factors. These latent factors construct the model by linearly combining the independent variables, and their weight coefficients are determined by minimizing the covariance between the predicted and true values. PLSR has significant advantages in dealing with high-dimensional data and small samples and is an essential tool in data modeling and analysis (Camarrone and

Van Hulle, 2019). PLSR has shown excellent predictive performance in several areas.

The input variable matrix and output variable matrix are decomposed:

$$X = DP^T + E \tag{17}$$

$$Y = UQ^T + F \tag{18}$$

Where  $X \in R^{N \times M}$ , is the input variable matrix,  $N$  is the number of samples, and  $M$  is the dimension of the input variable;  $D, U$  are the principal factor score matrices;  $P, Q$  are the loading matrices;  $E, F$  are the fitted residuals matrices; and  $Y \in R^{N \times K}$ , is the output variable matrix, and  $K$  is the dimension of the output variable.

The linear relationship between matrices  $D$  and  $U$  is:

$$U = DB \tag{19}$$

$$Y_{pre} = D_{pre}BQ \tag{20}$$

In Eq. (19) and Eq. (20),  $B = (D^T D)^{-1} D^T U$  is the regression coefficient matrix. After that, the training set data is inputted, and its principal factor score matrix  $D_{pre}$  is obtained according to Eq. (17). Then the output variable matrix  $Y_{pre}$  is obtained according to Eq. (20). By projecting the regression coefficient matrix, the regression model of PLSR can be obtained.

### 2.5.3 Support vector machines

SVM is a robust learning algorithm for classification and regression tasks. Its main goal is to find a hyperplane that can classify

data points into different fit data while maximizing the interval between the hyperplane and the nearest data points. SVM has excellent generalization performance, robustness, and applicability and is particularly suitable for dealing with high-dimensional, complex, or nonlinear datasets (Jain and Rastogi, 2022).

Define the training set  $Q = \{(x_i, y_i) | i = 1, 2, \dots, N\}$ , where  $x_i$  is 4-dimensional as the input vector,  $y_i$  is the output vector, and  $N$  is the total number of samples. Taking the quadratic sum of the error  $e$  as the loss function, the SVM optimization problem can be expressed as (Ashtiani et al., 2020):

$$\min_{w,s,e} J(w,e) = \frac{1}{2} w^T w + \frac{1}{2} \lambda \sum_{i=1}^N e_i^2 \quad (21)$$

$$s.t. y_i = w^T \cdot \varphi(x_i) + s + e_i \quad (22)$$

Where  $w$  is the weight variable;  $\lambda$  is the regularization parameter, here 100;  $s$  is the threshold;  $e_i$  is the error value;  $\varphi(x_i)$  is a nonlinear mapping in the kernel space. The original problem is transformed into the problem of finding the great value of the multiplier  $a_i$  according to the Lagrange multiplier method, and the following function is constructed:

$$L(w,s,e,\alpha) = J(w,e) - \sum_{i=1}^N \alpha_i (w^T \varphi(x_i) + s + e_i - y_i) \quad (23)$$

The regression function of SVM is:

$$f(x) = \sum_{i=1}^N \alpha_i K(x, x_i) + s \quad (24)$$

Where  $x$  is the input vector in the training set;  $K$  is the kernel function, and the radial basis function with a simple and stable structure is chosen as the kernel function, and its expression is:

$$K(x, x_i) = \exp\left(-\frac{\|x - x_i\|^2}{2\sigma^2}\right) \quad (25)$$

Where  $\sigma^2$  is the width of the kernel function, according to Equation (24), to predict the real weight of the material.

## 2.6 System performance verification experiments

In the material moisture content online monitoring system based on the Kalman filter fusion algorithm, the upper computer was still Lenovo's Legion Y7000P computer. It was used to complete the collection of material moisture content information. In MATLAB software, the Kalman filter fusion algorithm was written, including of the following: the Kalman filter and BP neural network fusion model. The impingement distance should be input into the MATLAB software in advance given that the impingement distance may not be detected by the sensor. In addition,

TABLE 1 Parameter settings for validation experiments.

| Factor                    | Groups |      |     |
|---------------------------|--------|------|-----|
|                           | 1      | 2    | 3   |
| Air velocity (m/s)        | 8.4    | 15.5 | 5.3 |
| Impingement distance (mm) | 60     | 140  | 100 |
| Drying temperature (°C)   | 68     | 53   | 46  |

the material's initial weight and initial moisture content should be input into the MATLAB software to further calculate the real-time moisture content of the material when the real-time weight of the material was obtained by the Kalman filter fusion algorithm.

After completing the construction of the monitoring system, performance verification experiments were conducted, following the construction of the monitoring system. The drying experiments of jujube slices were carried out in three drying environments set at random to ensure the reliability of the results of the validation experiments. Three data groups were randomly collected in each drying experiment and input into the BP neural network fusion model to complete the moisture content detection. The time interval between each data acquisition group was greater than 15 min. After each data acquisition, the material tray was removed, and the material was weighed to determine the actual moisture content of the material according to the oven method in Section 2.2. The initial moisture content of the jujube pieces was  $51.98\% \pm 0.50\%$ .

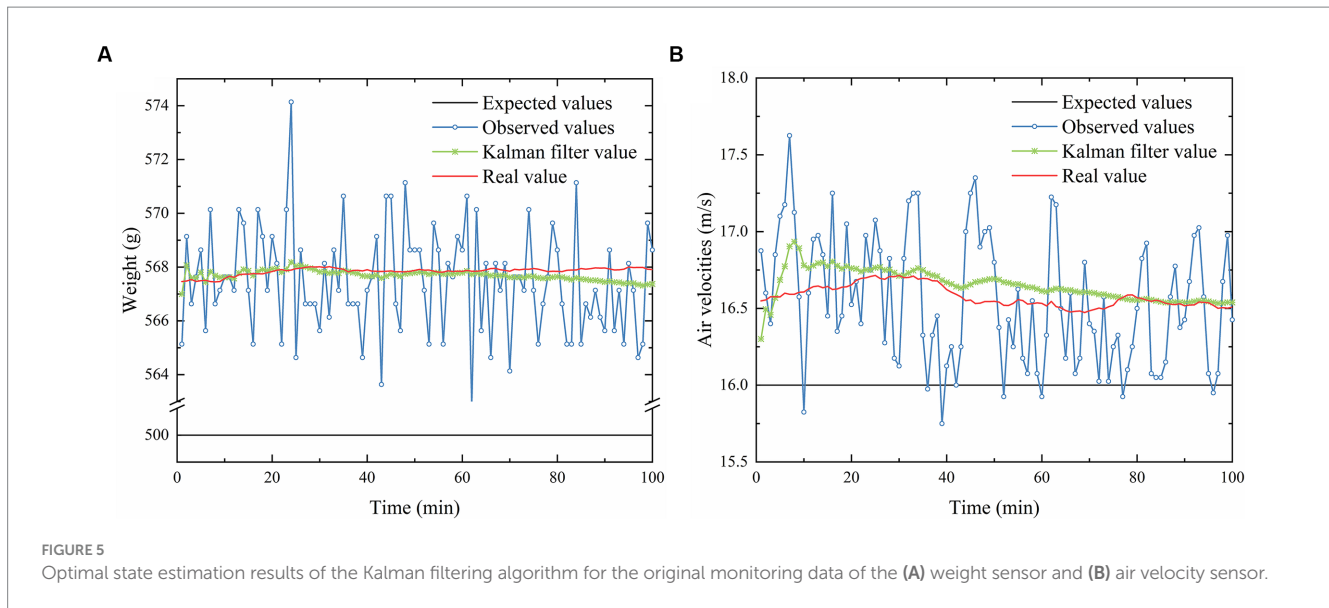
The setup parameters of the three drying environments are shown in Table 1. The air velocity refers to the air velocity of the air duct in the outer chamber, measured by the air velocity sensor in Figure 2. The sectional dimension of the air duct is 60 mm × 70 mm. The impingement distance refers to the distance between the air nozzle and the material, as shown in Figure 3. Drying temperature refers to the air temperature in the inner chamber, measured by the temperature sensor in Figure 1.

## 3 Results and discussion

### 3.1 Results and analysis of Kalman filter processing

Figure 5 illustrates the estimated optimal state of the weight and air velocity sensors using the Kalman filtering algorithm. The expected value refers to the detected index in the ideal state. The observed value was the original value acquired by the sensor. The Kalman filter value was the optimal estimate of the system state made by the Kalman filter algorithm. The real value was not the real state of the measured metric but the ideal value without bias. The two data sets were obtained under the same set of experiments, with 100 sampling points, and the sampling interval at both experiments was 1 min.

Figure 5A shows the optimal state estimation results of the Kalman filtering algorithm for the original monitoring data of the weight sensor under the conditions of drying temperature of 70 °C, wind speed of 16 m/s, and constant load of 500 g. The fluctuation range of the observed values was 562.1–574.1 g, and the fluctuation amplitude was 12 g. The optimal state estimation results of the Kalman filtering algorithm were consistent with the real values, and the overall tendency was stable. Experimental results indicated that the Kalman filtering algorithm adequately suppressed the noise and fluctuations in the original monitoring data of the weight sensor. A significant



error was found between the Kalman filtered value and the expected value, with a maximum error of 68.2 g. The detected value of the weighting sensor was affected by multiple factors other than the equipment vibration and the airflow disturbance, mainly the elastic substrate temperature and the air velocity. The experimental results also confirmed the need to establish a fusion model with multifactor inputs.

Figure 5B demonstrates the optimal estimation results of the Kalman filtering algorithm on the raw monitoring data of the air velocity sensor in the same set of experiments. The fluctuation range of the observed values was 15.75–17.63, and the fluctuation amplitude was 1.88 m/s. The Kalman filtered values of the air velocity sensor and the real values had evident fluctuations because the air velocity in the air-impingement dryer was open-loop control, and large fluctuations were observed in the wind speed. The air velocity of the centrifugal fan was controlled by adjusting the frequency of the inverter to realize the open-loop control, and the steady state error between the target value of air velocity and the output value was inevitable. Therefore, the Kalman-filtered and real values of the air velocity sensor had significant deviations from the expected value.

### 3.2 Pearson correlation analysis

Pearson correlation analysis of the four input variables and the detection error was conducted in this study to further quantitatively analyze the relationship between the weight detection value, elastic substrate temperature, airflow velocity, impingement distance, and the actual weight of the material. Detection error indicates the deviation between the detected value and the actual value of material weight. The results of the Pearson correlation analysis are shown in Figure 6.

The correlation between airflow velocity and detection error was as high as 0.811, suggesting that the leading cause was the airflow velocity. This result also proved the feasibility of using the air-stop detection scheme to detect the moisture content of the material in the existing studies. The positive correlation between air velocity and detection error

was caused by the effect of the airflow on the material tray from top to bottom. In addition, a large air velocity indicates large impact force of the airflow on the material tray and large detection.

The impingement distance negatively correlated with the detection error with a correlation coefficient of  $-0.357$ . The impingement distance represented the distance between the airflow nozzle and the tray. The larger distance indicates more dispersed airflow, smaller impact on the tray, and smaller detection error. The effect of the impingement distance on the detection error was highly dependent on the air velocity. When the air velocity is zero, the change in impingement distance does not affect the detection of material weight.

The temperature of the elastic substrate and the weight detection value were positively correlated with the detection error, with correlation coefficients of 0.226 and 0.329, respectively. In resistance strain pressure sensors, the pressure to be detected deforms the elastic substrate, which is transformed into a change in electrical resistance, thereby realizing the weight detection. The temperature significantly affected the resistance, exhibiting a positive correlation (Burnos and Rys, 2017). Therefore, when the temperature of the elastic substrate was high, the detection value of the weighting sensor was large, as well as the detection error.

The weight detection value and the detection error are correlated because the effect of temperature on the detection error was related to the load of the weighting sensor. The relationship between temperature and detection error was different at varied load intervals. The weight detection value had the most direct relationship with load; thus, the effect of temperature on the detection error resulted in the correlation between the weight detection value and the detection error. Wang et al. (2014) has linearly corrected the detection value of the weighing sensor in different subtemperature segments and subload segments.

### 3.3 Training results and analysis of BP neural network fusion models

After confirming the correlation between the weight detection value, elastic substrate temperature, airflow velocity, and impingement

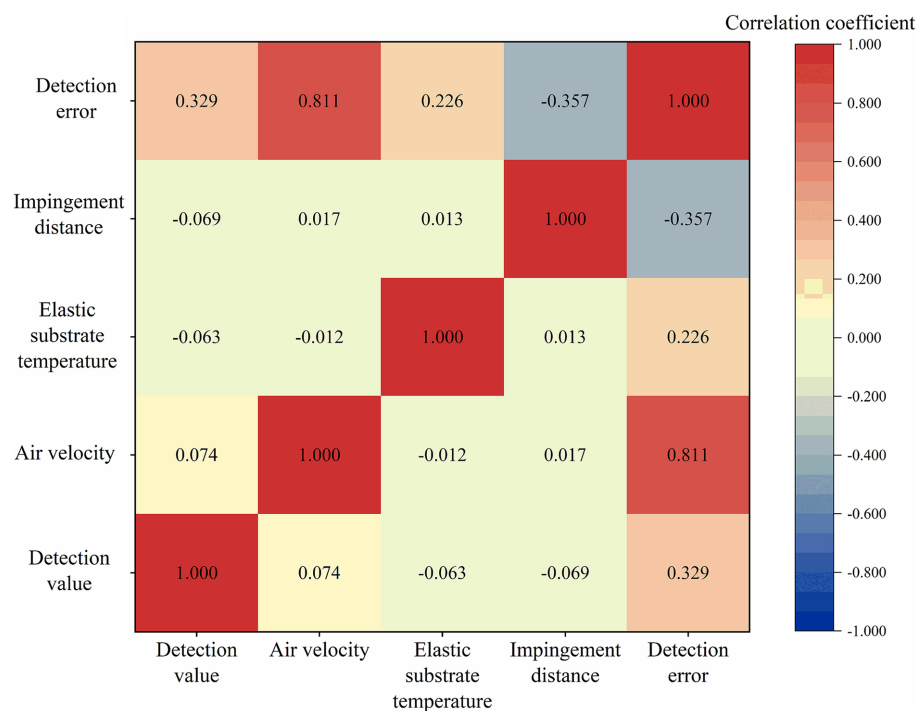


FIGURE 6 Results of Pearson correlation analysis.

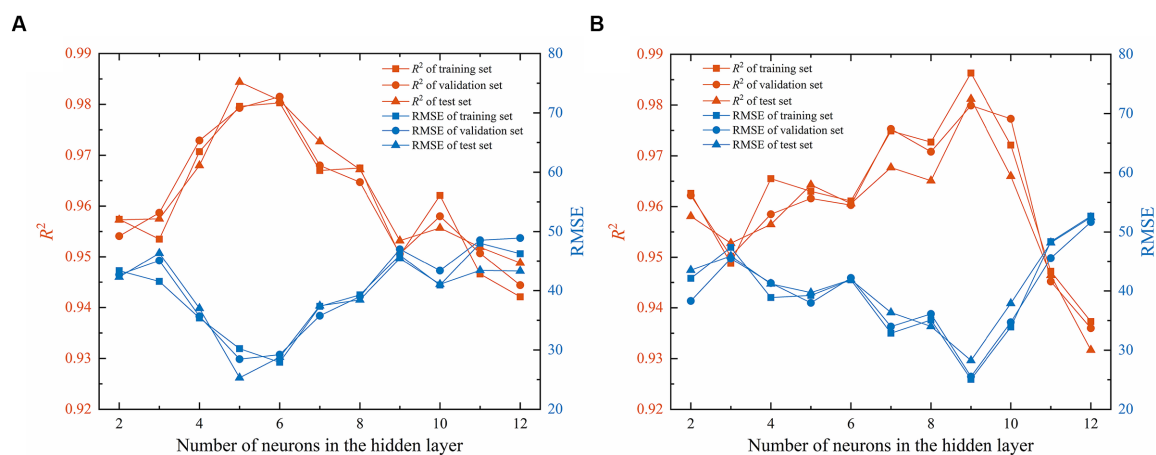


FIGURE 7 Prediction results for the test set of BP neural network fusion models. The fitting plot (A) and error plot (B) of the predicted and actual values of the test set.

distance on the true weight of the material, the four input variables were fused to establish a BP neural network fusion model with the actual weight of the material as the output.

### 3.3.1 Optimal topology selection

Test experiments were conducted for different activation functions and the number of neurons in the hidden layer to obtain the optimal topology of the BP neural network. The test results are shown in Figure 7. The uncertainty of the test results was large because the initial weights and thresholds of the current BP neural network were randomly generated. Thus, the results of

the test experiments were considered the average of 10 test trials. The learning rate of the training process of the BP neural network was 0.001, and the maximum number of iterations was 150.

Figure 7A shows the RMSE and  $R^2$  of the three data sets with different numbers of neurons in the hidden layer under the condition that the activation function between the input layer and the hidden layer was Tansig. The RMSE of all three datasets roughly showed a tendency to decrease and then increase, and it reached the lowest point when the number of neurons in the hidden layer was 5. The  $R^2$  of all three datasets showed a trend of increasing and then decreasing, reaching the highest point when

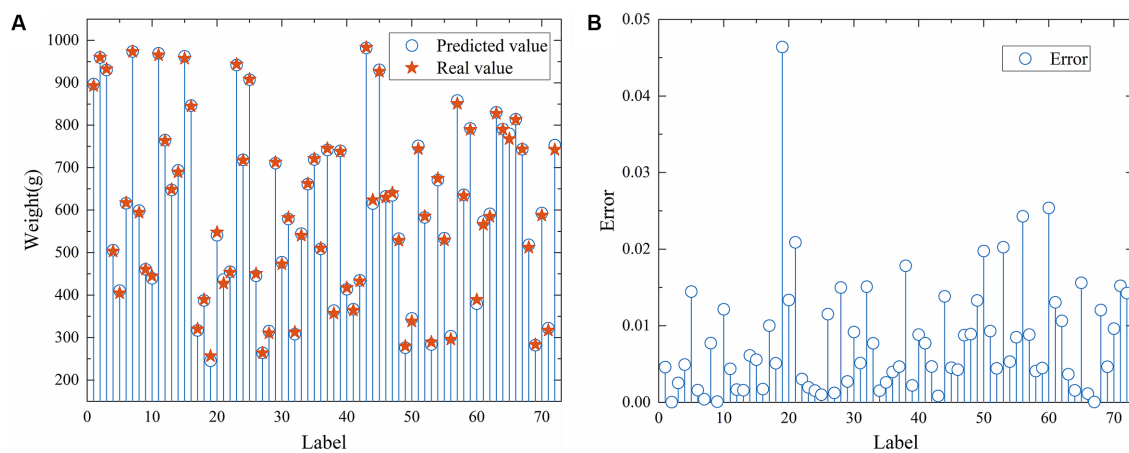


FIGURE 8

Test results for different topologies. The RMSE and  $R^2$  of the three data sets with different numbers of neurons under the condition that the activation function were Tansig (A) and Logsig (B).

the number of nodes in the hidden layer was 5. This finding was because of the inability of the topology of the neural network to satisfy the requirements of the training dataset when the number of neurons was extremely small, thereby reducing the model's accuracy. When the number of nodes was extremely high, the network was highly susceptible to overfitting, which decreased the model's accuracy (Yang et al., 2023). When the number of neurons in the hidden layer was 5, the RMSE and  $R^2$  of the test set were 0.9844 and 25.3, respectively.

Figure 7B shows the RMSE and  $R^2$  for three data sets with different numbers of neurons in the hidden layer. The activation function was Logsig between the input layer and the hidden layer. Figure 7B shows approximately the same pattern as Figure 7A, except that the optimal neuron number was 9, and the RMSE and  $R^2$  of the test set were 0.9812 and 28.3, respectively. After comprehensively comparing the RMSE and  $R^2$  for the two optimal neuron numbers, we obtained the optimal topology of the BP neural network with the activation function between the input layer and the hidden layer, which was Tansig. Moreover, the number of neurons in the hidden layer was 5.

### 3.3.2 Genetic algorithm optimization

After determining the optimal topology of the BP neural network, the model's training results were still unsatisfactory because the initial weights and thresholds of the neural network were randomly generated. This randomness results in local optimal training results, but not the global optimal. Figure 8 shows the training results after the genetic algorithm optimized the initial weights and thresholds of the BP neural network. The RMSE and  $R^2$  of the test set were 4.9 and 0.9995, respectively, and the RMSE was reduced by 80.6% compared with the preoptimization. Figure 8A shows the fitting plot of the predicted and actual values of the test set, and the model had an excellent prediction effect. Figure 8B demonstrates the error plot of the test set's predicted and actual values. The maximum error within the permissible range of the online monitoring system for moisture content was 0.046.

## 3.4 Model performance comparison

Figures 9A–C show the scatter plots of the three datasets of PLSR, SVM, and BP neural networks, respectively. The scatter points of the BP neural network fusion model were more centrally distributed near the regression line than those of the two other models. The PLSR and SVM models showed satisfactory prediction results, but the RMSEs of the two prediction models were 41.4 and 39.2, which cannot satisfy the accuracy requirements of the online moisture content monitoring system. Although the structure and topology of the BP neural network are more complex compared to the other two models, collectively, the excellent prediction results of the BP neural network indicate that it can better capture the complex nonlinear relationship between the inputs and the outputs, and is also more suitable for online detection of moisture content. Each prediction model and structure has its applicable scenarios and limitations. Selecting a prediction model and structure depends on the problem and data characteristics in practical applications.

## 3.5 Validation experiment results and analysis

Table 2 shows the results of the validation experiments of the moisture content online monitoring system. The  $R^2$  value of the nine sets of validation experiments was 0.9963, which was smaller than the  $R^2$  of the weight fusion model (0.9995). A more significant uncertainty in the material moisture content detection than the material weight detection was observed. The moisture content detection based on the weighing method was based on the premise that the moisture content of the same batch of materials was the same. The samples used for the moisture content detection in the oven method always had error with the materials in the actual drying process, thereby increasing the material moisture content detection error. Nine groups of validation experiments had an RMSE of 0.78, and the maximum error was 6.27. The results of the validation experiments indicate that the online monitoring system of moisture content satisfies

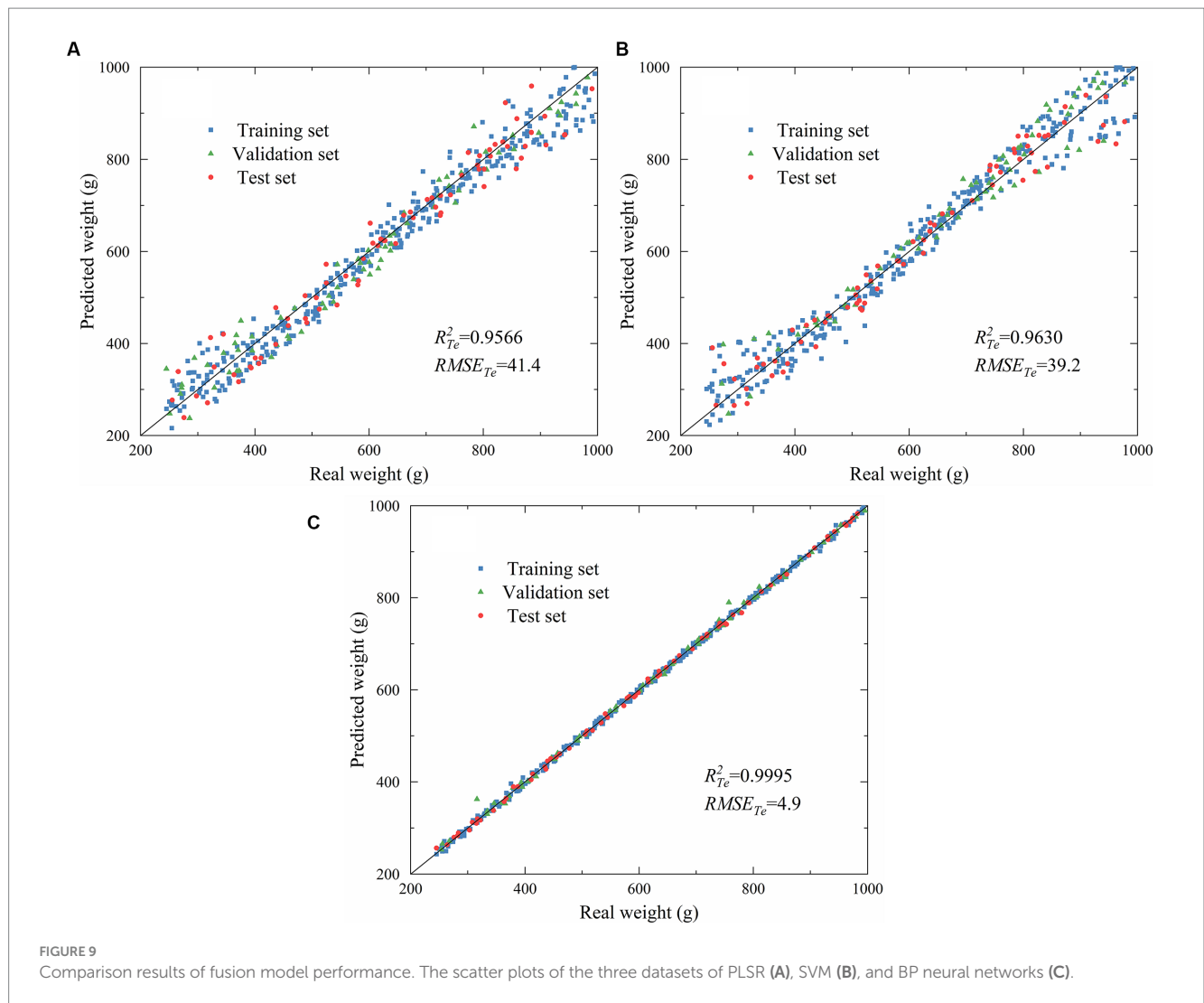


TABLE 2 Results of validation experiments.

| Groups                         | 1     |       |       | 2     |       |       | 3     |       |       | $R^2$  | RMSE |
|--------------------------------|-------|-------|-------|-------|-------|-------|-------|-------|-------|--------|------|
| Number                         | 1     | 2     | 3     | 1     | 2     | 3     | 1     | 2     | 3     |        |      |
| True moisture content (%)      | 39.51 | 17.28 | 12.53 | 45.18 | 20.92 | 11.32 | 37.83 | 16.42 | 10.6  | 0.9963 | 0.78 |
| Predicted moisture content (%) | 38.48 | 17.89 | 13.21 | 44.42 | 20.09 | 11.99 | 38.62 | 17.45 | 10.98 |        |      |
| Error (%)                      | 2.61  | 3.53  | 5.43  | 1.68  | 3.97  | 5.92  | 2.09  | 6.27  | 3.58  |        |      |

the accuracy requirements of moisture content detection in the drying process.

### 4 Conclusion

An information acquisition system of material moisture content was developed, and the raw data used to establish the Kalman filter fusion algorithm were obtained. The Kalman filter processing was carried out on the raw detection values of the weight sensor and air velocity sensor, and the optimal state estimation of the weight detection value and air velocity was obtained. The information

fusion processing of weight detection value, elastic substrate temperature, airflow velocity, and impingement distance was carried out using the estimated value, and the BP neural network fusion model with material weight as the output was established. The optimal topology of the BP neural network fusion model was selected; the activation function is Tansig, Pureline, and the number of neurons in the hidden layer is 5. The initial weights and thresholds of the BP neural network were optimized using genetic algorithms. The  $R^2$  and RMSE of the test set of the optimized fusion model were 0.9995 and 4.9, respectively, and the RMSE was reduced compared with the preoptimization by 80.6%. Fusion models based on PLSR and SVM were also developed and compared with the BP

neural network fusion model. The accuracy of the BP neural network model was significantly better than the two other models. An online moisture content monitoring system was constructed using the Kalman filter fusion algorithm, and validation experiments were carried out for the detection accuracy of the system. The  $R^2$  and RMSE of the nine groups of validation experiments were 0.9963 and 0.78, respectively, indicating that the monitoring system satisfies the accuracy requirements of the material moisture content detection in the drying process. This study provides technical support for optimizing the drying process based on the change in moisture content, as well as a reference for online monitoring of moisture content in other drying equipment.

## Data availability statement

The raw data supporting the conclusions of this article will be made available by the authors, without undue reservation.

## Author contributions

TY: Conceptualization, Data curation, Formal analysis, Investigation, Methodology, Software, Validation, Visualization, Writing – original draft, Writing – review & editing. XZ: Conceptualization, Formal analysis, Investigation, Project administration, Supervision, Validation, Writing – review & editing. HX: Validation, Writing – review & editing. CS:

Validation, Writing – review & editing. JZ: Validation, Writing – review & editing.

## Funding

The author(s) declare financial support was received for the research, authorship, and/or publication of this article. This study was supported by the Shihezi University Achievement Transformation and Technology Promotion Project (No. CGZH201808).

## Conflict of interest

The authors declare that the research was conducted in the absence of any commercial or financial relationships that could be construed as a potential conflict of interest.

## Publisher's note

All claims expressed in this article are solely those of the authors and do not necessarily represent those of their affiliated organizations, or those of the publisher, the editors and the reviewers. Any product that may be evaluated in this article, or claim that may be made by its manufacturer, is not guaranteed or endorsed by the publisher.

## References

- Ashtiani, S. H. M., Rohani, A., and Aghkhani, M. H. (2020). Soft computing-based method for estimation of almond kernel mass from its shell features. *Sci. Hortic.* 262:109071. doi: 10.1016/j.scienta.2019.109071
- Burnos, P., and Rys, D. (2017). The effect of flexible pavement mechanics on the accuracy of axle load sensors in vehicle weigh-in-motion systems. *Sensors* 17:2053. doi: 10.3390/s17092053
- Camarrone, F., and Van Hulle, M. M. (2019). Fast multiway partial least squares regression. *IEEE Trans. Biomed. Eng.* 66, 433–443. doi: 10.1109/tbme.2018.2847404
- Celik, E., Parlak, N., and Cay, Y. (2022). Development of an integrated corn dryer with an indirect moisture measuring system. *Sadhana-academy proceedings. Eng. Sci.* 47, 1–8. doi: 10.1007/s12046-021-01775-1
- Chang, A., Zheng, X., Xiao, H., Yao, X., Liu, D., Li, X., et al. (2022). Short- and medium-wave infrared drying of cantaloupe (*Cucumis melon* L.) slices: drying kinetics and process parameter optimization. *PRO* 10:114. doi: 10.3390/pr10010114
- Cho, J.-S., Choi, J.-Y., and Moon, K.-D. (2020). Hyperspectral imaging technology for monitoring of moisture contents of dried persimmons during drying process. *Food Sci. Biotechnol.* 29, 1407–1412. doi: 10.1007/s10068-020-00791-x
- Dalvi-Isfahan, M. (2020). A comparative study on the efficiency of two modeling approaches for predicting moisture content of apple slice during drying. *J. Food Process Eng.* 43:e13527. doi: 10.1111/jfpe.13527
- Espinoza-Espinoza, L. A., Juarez-Ojeda, C. E., Ruiz-Flores, L. A., Moreno-Quispe, L. A., Anaya-Palacios, M. S., and Cardenas-Quintana, H. (2023). Influence of convection drying with hot air on the physicochemical and phytochemical properties of green banana flour (*Musa cavendish*). *Frontiers in Sustainable Food Systems* 7:1204349. doi: 10.3389/fsufs.2023.1204349
- Jain, S., and Rastogi, R. (2022). Parametric non-parallel support vector machines for pattern classification. *Mach. Learn.* doi: 10.1007/s10994-022-06238-0
- Ji, H., Yang, F., Wang, Z., Hu, X., Qi, A., Lv, B., et al. (2023). Research on wear state identification and life prediction technology of ultrasonic straight-edge knife. *Int. J. Adv. Manuf. Technol.* 127, 4225–4235. doi: 10.1007/s00170-023-11727-0
- Ju, H.-Y., Vidyarthi, S. K., Karim, M. A., Yu, X.-L., Zhang, W.-P., and Xiao, H.-W. (2023). Drying quality and energy consumption efficient improvements in hot air drying of papaya slices by step-down relative humidity based on heat and mass transfer characteristics and 3D simulation. *Dry. Technol.* 41, 460–476. doi: 10.1080/07373937.2022.2099416
- Kalathingal, M. S. H., Basak, S., and Mitra, J. (2020). Artificial neural network modeling and genetic algorithm optimization of process parameters in fluidized bed drying of green tea leaves. *J. Food Process Eng.* 43:e13128. doi: 10.1111/jfpe.13128
- Li, M., Ai, Z., Xiao, H., Mowafy, S., Pei, Y., and Liu, Y. (2023). Improvement of drying efficiency and physicochemical quality of kiwifruit slices using infrared-assisted tilted tray air impingement drying. *Dry. Technol.* 41, 1159–1170. doi: 10.1080/07373937.2022.2125526
- Li, L., Chen, J., Duan, X., and Ren, G. (2021). Prediction model for moisture content in cantaloupe slices using LF-NMR and different drying methods. *Transactions of the Chinese Society of Agricultural Engineering* 37, 304–312. doi: 10.11975/j.issn.1002-6819.2021.2.035
- Li, H., Yan, L., and Xia, Y. (2022). Distributed robust Kalman filtering for Markov jump systems with measurement loss of unknown probabilities. *Ieee Transactions on Cybernetics* 52, 10151–10162. doi: 10.1109/tycb.2021.3062641
- Liu, Z.-L., Bai, J.-W., Wang, S.-X., Meng, J.-S., Wang, H., Yu, X.-L., et al. (2020). Prediction of energy and exergy of mushroom slices drying in hot air impingement dryer by artificial neural network. *Dry. Technol.* 38, 1959–1970. doi: 10.1080/07373937.2019.1607873
- Liu, Z.-L., Wei, Z.-Y., Vidyarthi, S. K., Pan, Z., Zielinska, M., Deng, L.-Z., et al. (2020). Pulsed vacuum drying of kiwifruit slices and drying process optimization based on artificial neural network. *Dry. Technol.* 39, 405–417. doi: 10.1080/07373937.2020.1817063
- Liu, D., Zheng, X., Xiao, H., Yao, X., Shan, C., Chang, A., et al. (2021). Optimization of sequential freeze-infrared drying process. *Transactions of the Chinese society of Agric. Eng.* 37:293–302. doi: 10.11975/j.issn.1002-6819.2021.17.034
- Martin, T.H., and Howard, B.D. (2002). *Neural network design. 2nd(Edn)*. Beijing, China: China Machine Press.
- Peng, J., Yin, X., Jiao, S., Wei, K., Tu, K., and Pan, L. (2019). Air jet impingement and hot air-assisted radio frequency hybrid drying of apple slices. *Lwt-Food Science and Technology* 116:108517. doi: 10.1016/j.lwt.2019.108517
- Pongsuttiyakorn, T., Sooraksa, P., and Pornchalermpong, P. (2019). Simple effective and robust weight sensor for measuring moisture content in food drying process. *Sensors and Materials* 31, 2393–2404. doi: 10.18494/sam.2019.2347
- Raj, G. V. S. B., and Dash, K. K. (2020). Microwave vacuum drying of dragon fruit slice: artificial neural network modelling, genetic algorithm optimization, and kinetics study. *Comput. Electron. Agric.* 178:105814. doi: 10.1016/j.compag.2020.105814
- Reyer, S., Awiszus, S., and Muller, J. (2022). High-precision laboratory dryer for characterization of the drying behavior of agricultural and food products. *Mach. Des.* 10:10050372. doi: 10.3390/machines10050372

- Tan, S., Miao, Y., Xiang, H., Tan, W., and Li, W. (2021). Effects of air-impingement jet drying on drying kinetics and quality retention of tomato slices. *Food Sci. Biotechnol.* 30, 691–699. doi: 10.1007/s10068-021-00904-0
- Tan, S., Wang, Y., Fu, W., Luo, Y., Cheng, S., and Li, W. (2022). Drying kinetics and physicochemical properties of kumquat under hot air and air-impingement jet dryings. *Food Sci. Biotechnol.* 31, 711–719. doi: 10.1007/s10068-022-01080-5
- Wang, D., Lin, H., Xiao, H., Liu, Y., Ju, H., Dai, J., et al. (2014). Design of online monitoring system for material moisture content in air-impingement drying process. *Transactions of the Chinese Society of Agricultural Engineering* 30, 316–324. doi: 10.3969/j.issn.1002-6819.2014.19.038
- Wang, J., Lu, Z., Wang, G., Hussain, G., Zhao, S., Zhang, H., et al. (2023). Research on fault diagnosis of HMCVT shift hydraulic system based on optimized BPNN and CNN. *Agriculture-Basel* 13:461. doi: 10.3390/agriculture13020461
- Wang, J., Xiao, H.-W., Fang, X.-M., Mujumdar, A. S., Vidyarthi, S. K., and Xie, L. (2022). Effect of high-humidity hot air impingement blanching and pulsed vacuum drying on phytochemicals content, antioxidant capacity, rehydration kinetics and ultrastructure of Thompson seedless grape. *Dry. Technol.* 40, 1013–1026. doi: 10.1080/07373937.2020.1845721
- Xiao, H.-W., and Mujumdar, A. S. (2020). Importance of drying in support of human welfare. *Dry. Technol.* 38, 1542–1543. doi: 10.1080/07373937.2019.1686476
- Xie, Y., Lin, Y., Zhu, G., Yu, X., Xue, L., Gao, Z., et al. (2018). Structure optimization and experiment of radio frequency dryer based on heating uniformity. *Transactions of the Chinese Society of Agricultural Engineering* 34, 248–255. doi: 10.11975/j.issn.1002-6819.2018.05.033
- Xue, L., Wang, S., Gao, Z., Yu, X., Lin, H., and Wei, Q. (2018). On-line measurement of material quality in vacuum drying process. *Transactions of the Chinese Society for Agricultural Machinery* 49, 326–337. doi: 10.6041/j.issn.1000-1298.2018.09.038
- Yang, H., Li, H., Xia, Y., and Li, L. (2021). Distributed Kalman filtering over sensor networks with transmission delays. *Ieee Transactions on Cybernetics* 51, 5511–5521. doi: 10.1109/tcyb.2020.2980582
- Yang, M., Liu, E., Wu, Y., Yang, S., Yang, L., Pu, Y., et al. (2023). Development and experiments of an online moisture content measuring device in thin layer hot-air drying process. *Transactions of the Chinese Society of Agricultural Engineering* 39, 47–56. doi: 10.11975/j.issn.1002-6819.202211176
- Yang, T., Zheng, X., Vidyarthi, S. K. K., Xiao, H., Yao, X., Li, Y., et al. (2023). Artificial neural network modeling and genetic algorithm multiobjective optimization of process of drying-assisted walnut breaking. *Foods* 12:1897. doi: 10.3390/foods12091897
- Yang, T., Zheng, X., Xiao, H., Shan, C., Yao, X., Li, Y., et al. (2023). Drying temperature precision control system based on improved neural network PID controller and variable-temperature drying experiment of cantaloupe slices. *Plants-Basel* 12:2257. doi: 10.3390/plants12122257
- You, S. H., Ahn, C. K., Zhao, S., and Shmaliy, Y. S. (2022). Frobenius norm-based unbiased finite impulse response fusion filtering for wireless sensor networks. *IEEE Trans. Ind. Electron.* 69, 1867–1876. doi: 10.1109/tie.2021.3055172
- Zahoor, I., Anjum, N., Ganaie, T. A., Allai, F. M., Al-Ghamdi, A. A., Abbasi, A. M., et al. (2022). Effect of hybrid drying technique on non-traditional chicory (*Cichorium intybus* L.) herb: phytochemical, antioxidant characteristics, and optimization of process conditions. *Frontiers in Sustainable Food Systems* 6:1002396. doi: 10.3389/fsufs.2022.1002396
- Zartha Sossa, J. W., Orozco, G. L., Garcia Murillo, L. M., Pena Osorio, M., and Sanchez Suarez, N. (2021). Infrared drying trends applied to fruit. *Frontiers in Sustainable Food Systems* 5:650690. doi: 10.3389/fsufs.2021.650690
- Zheng, Y., Li, L., Qian, L., Cheng, B., Hou, W., and Zhuang, Y. (2023). Sine-SSA-BP ship trajectory prediction based on chaotic mapping improved sparrow search algorithm. *Sensors* 23:704. doi: 10.3390/s23020704